Dynamics of the seasonal variation of the North Equatorial Current bifurcation

Zhaohui Chen[1] and Lixin Wu[1]

Received 16 September 2010; revised 9 November 2010; accepted 30 November 2010; published 15 February 2011.

[1] The dynamics of the seasonal variation of the North Equatorial Current (NEC) bifurcation is studied using a 1.5-layer nonlinear reduced-gravity Pacific basin model and a linear, first-mode baroclinic Rossby wave model. The model-simulated bifurcation latitude exhibits a distinct seasonal cycle with the southernmost latitude in June and the northernmost latitude in November, consistent with observational analysis. It is found that the seasonal migration of the NEC bifurcation latitude (NBL) not only is determined by wind locally in the tropics, as suggested in previous studies, but is also significantly intensified by the extratropical wind through coastal Kelvin waves. The model further demonstrates that the amplitude of the NEC bifurcation is also associated with stratification. A strong (weak) stratification leads to a fast (slow) phase speed of first-mode baroclinic Rossby waves, and thus large (small) annual range of the bifurcation latitude. Therefore, it is expected that in a warm climate the NBL should have a large range of annual migration.

Citation: Chen, Z., and L. Wu (2011), Dynamics of the seasonal variation of the North Equatorial Current bifurcation, *J. Geophys. Res.*, *116*, C02018, doi:10.1029/2010JC006664.

1. Introduction

[2] The North Equatorial Current (NEC) in the western Pacific bifurcates as it encounters the Philippine coast, separating into two branches, which are the northward flowing Kuroshio and southward flowing Mindanao Current (MC) [*Nitani*, 1972]. This partition of the water mass as well as the heat transport between the poleward and equatorward flows, not only has a great influence upon the low-latitude western boundary currents, but is also believed to be important in determining the interactions between the atmosphere and ocean [*Lukas et al.*, 1996]. Early synoptic observations provided a general description of the NEC bifurcation [*Wyrtki*, 1961; *Nitani*, 1972; *Toole et al.*, 1988, 1990; *Qu et al.*, 1998], but observational evidence as well as our understanding of the dynamics of the seasonal variation of the NEC bifurcation latitude (NBL) remains incomplete.

[3] Based on a synthesis of historical temperature and salinity data, *Qu and Lukas* [2003] demonstrated that the NBL occurs at the southernmost position in July and the northernmost position in December. They suggested that the seasonal bifurcation migration corresponds well with the local Ekman pumping associated with the Asian monsoonal winds. The results are also supported by a high-resolution ocean general circulation model [*Kim et al.*, 2004] and recent observational data analysis [*Wang and Hu*, 2006; *Qiu and Chen*, 2010]. Using a reduced-gravity, primitive equation OGCM, *Rodrigues et al.* [2007] also pointed out local forcing is more important than the remote forcing (i.e., westward propagation of anomalies) on the seasonal variation of the South Equatorial Current bifurcation in the Atlantic Ocean.

[4] The study of *Qiu and Lukas* [1996] (hereinafter referred to as QL96) laid an important foundation for understanding the dynamics of the NBL seasonal variability using linear time-dependent Sverdrup theory. However, as *Qu and Lukas* [2003] pointed out, the phase and amplitude of the NBL seasonal variation predicted by the linear wave dynamics appear to be different from observations and the nonlinear reduced-gravity model simulation. The amplitude predicted by the linear Sverdrup theory only accounts for half of that in the nonlinear reduced-gravity model simulation, and the time to reach its southernmost position appears to be 2–3 months earlier than the later. Are these differences associated with nonlinearity and/or wind stress forcing outside of the tropics, in particular the extratropical wind stress forcing which was not included in the linear Sverdrup theory? Furthermore, although the phase of the NBL in different observational data analysis appears to be fairly consistent, the peak-to-peak amplitude displays a large deviation ranging from 1° to 2.5° (Figure 1). The discrepancies in the NBL seasonal variation may be partly associated with different data used in individual studies, methods to define the bifurcation latitude as well as the NBL dependence on the depth, but also require a further understanding of the dynamics in governing the seasonal migration of the NBL.

[5] The questions above motivate us to further examine the dynamics in controlling the NBL seasonal variation, with special focus on the relative importance of the extratropical versus tropical wind stress forcing and baroclinic Rossby wave propagation. We use a 1.5-layer Pacific basin model and a linear, first-mode baroclinic Rossby wave model together with observations and OGCM model simulations to systematically explore these dynamic effects. It is found that

[1]Physical Oceanography Laboratory, Ocean University of China, Qingdao, China.

0148-0227/11/2010JC006664

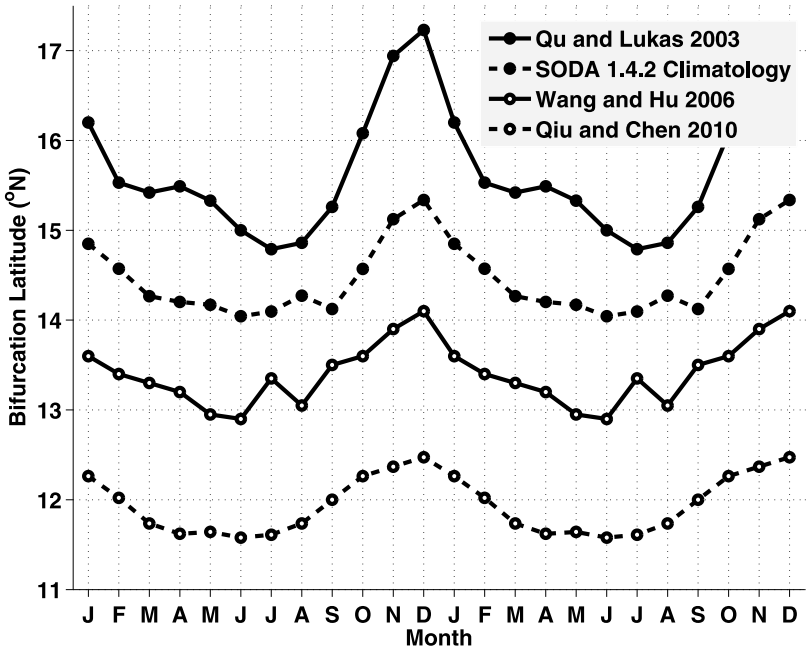

Figure 1. Seasonal variation of the NBL derived from the historical climatology, ocean reanalysis product, and the *T*/*P* altimetry data by different studies.

these dynamic effects can regulate both the phase and amplitude of the NBL seasonal variation.

[6] This paper is organized as follows. Section 2 gives a brief description of the seasonal variation of the NEC bifurcation simulated by a 1.5-layer nonlinear reduced-gravity model. In section 3, a detailed examination of the wind stress in the extratropics in controlling the seasonal variation of the NEC bifurcation is presented. Role of baroclinic Rossby wave propagation in the seasonal variation of the NEC bifurcation is presented in section 4, followed by some discussions in section 5. Section 6 summarizes the results.

2. Seasonal Variation of the NBL in a 1.5-Layer Pacific Basin Model

[7] Previous studies indicated that the wind stress plays a dominant role in determining the bifurcation of a lower-latitude zonal jet with thermodynamic effect playing only a minor role [*Rodrigues et al.*, 2007]. Here we use a 1.5-layer nonlinear reduced-gravity Pacific basin model forced by wind stress only to study the seasonal variation of the NEC bifurcation.

[8] The governing equations can be written as

$$\frac{\partial u}{\partial t}+u\frac{\partial u}{\partial x}+v\frac{\partial u}{\partial y}-fv+g'\frac{\partial h}{\partial x}=A_H\nabla^2 u+\frac{\tau^x}{\rho(H+h)}, \quad (1)$$

$$\frac{\partial v}{\partial t}+u\frac{\partial v}{\partial x}+v\frac{\partial v}{\partial y}+fu+g'\frac{\partial h}{\partial y}=A_H\nabla^2 v+\frac{\tau^y}{\rho(H+h)}, \quad (2)$$

$$\frac{\partial h}{\partial t}+H\left(\frac{\partial u}{\partial x}+\frac{\partial v}{\partial y}\right)=0, \quad (3)$$

where u and v is the zonal and meridional velocity, h the upper layer thickness deviation, H the mean upper layer thickness, f the Coriolis parameter, g' the reduced-gravity acceleration, A_H the coefficient of horizontal eddy viscosity, ρ the reference water density, τ^x and τ^y the surface wind stress. The horizontal resolution in this model is 1/4°, and the domain covers the subtropical and tropical region in the north Pacific, which extends from 20°S to 40°N in the meridional direction and 120°E to the American coast in the zonal direction. Marginal seas shallower than 600 m are treated as land. In the model, the Luzon Strait which connects the South China Sea (SCS) and the western Pacific is closed. This type of model configuration blocks coastal Kelvin waves (CKWs) from the extratropical basin coasts to the SCS, but will not change our conclusions qualitatively. This will be discussed in section 5.

[9] No normal flow and nonslip boundary conditions are used along the coast but with free-slip condition applied to the northern and southern open boundaries. From 30°N to 40°N, A_H increases linearly from 2000 $m^2\ s^{-1}$ to 6000 $m^2\ s^{-1}$ for the purpose of suppressing instabilities in the Kuroshio extension regions and damping spurious CKWs along the artificial northern boundary. The density contrast between the infinite ocean (ρ = 1025 kg m^{-3}) and the upper layer ocean $\Delta\rho$ = 3 kg m^{-3} and the initial upper layer thickness H = 350 m, thus the phase speed of the first-mode baroclinic Rossby wave is approximately 0.16 m s^{-1} which is consistent with the observational study around the bifurcation latitude [*Chelton and Schlax*, 1996; *Chelton et al.*, 1998].

[10] The model is first spun up from rest by the European Centre for Medium-Range Weather Forecasts (ECMWF) Reanalysis (ERA40) climatological wind stress for 20 years. After the spin-up, the model is forced by the monthly climatological wind stress for an additional 24 years as the control run. The climatological and seasonally varying wind

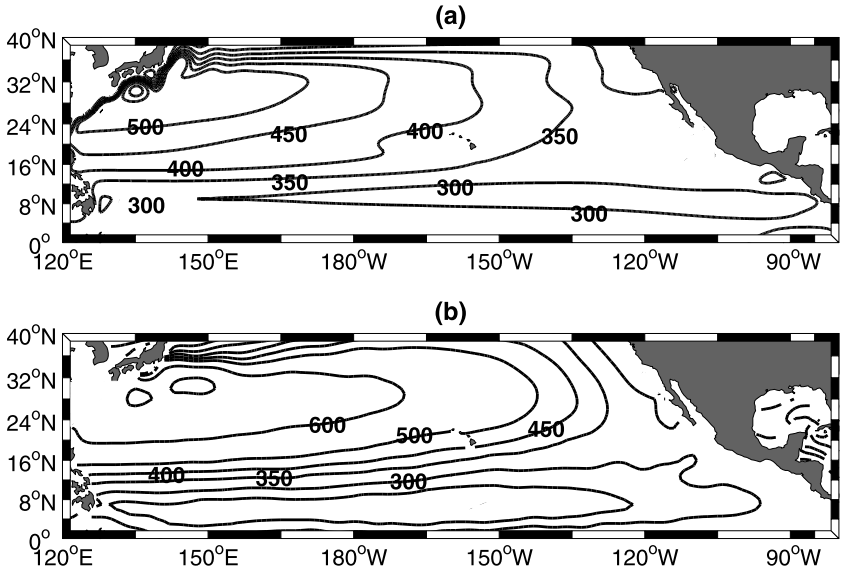

Figure 2. (a) Mean upper layer thickness (m) averaged from the last 12 years' control run. (b) Depth of the 26.7 σ_θ surface (m) based on the *World Ocean Atlas* 2009 (WOA09) climatological data sets of temperature and salinity.

stress are both derived from the daily wind stress data set spanning from 1978 to 2001 of the ERA40.

[11] The model simulated mean upper layer thickness is displayed in Figure 2a. For comparison, the depth of 26.7 σ_θ surface (Figure 2b) is derived from the WOA09 climatological data sets of temperature and salinity [*Locarnini et al.*, 2010; *Antonov et al.*, 2010]. The upper layer thickness in the model agrees broadly with the observed thermocline, which deepens toward the west with the maximum located in the recirculation gyre of the subtropical basin. Both the subtropical gyre and the tropical region circulation are captured, although the subtropical component north of 30°N is poorly simulated due to artificial northern boundary. In the tropical Pacific, the model reasonably captures the thermocline depth in the bifurcation region as well as in the Mindanao Dome region [*Masumoto and Yamagata*, 1991]. As pointed by *Qu et al.* [1998], the NEC bifurcation is mainly confined between the surface and the 26.7 σ_θ isopycnal, and this depth represents the interface between the upper and lower thermocline, thus, is a good proxy for the thermocline in the western Pacific.

[12] The seasonal migration of the NBL in the model is demonstrated in Figure 3. Here the NBL is derived by following the method of QL96. In their study, the NBL is defined as the latitude where the averaged meridional flow 2° band off the Philippine coast is zero. This method has been also used by *Qu and Lukas* [2003] and *Kim et al.* [2004]. The annual mean latitude occurs at 14.7°N, which is about 1° south of that shown by *Qu and Lukas* [2003] and 1° north of that by *Wang and Hu* [2006]. Since the NBL displays a northward shift with increasing depth [*Nitani*, 1972], this discrepancy is likely due to the fact that the NBL defined by *Qu and Lukas* [2003] is the average in the upper 1000 m while the NBL in the model represents an average of the upper 400 m near the Philippine coast. It has been suggested that the northward migration of the bifurcation latitude with increasing depth is associated with the interaction between the Sverdrup transport and boundary conditions on density [*Reid and Arthur*, 1975] and the conservation of the potential vorticity [*Toole et al.*, 1990].

[13] For the seasonal variation, the model simulated NBL reaches the southernmost latitude in June and the northernmost latitude in November, consistent with observations. The model-simulated NBL magnitude is about 2° within the range of the observations. For comparisons, we also calculate the seasonal NBL from the climatological meridional velocity of the Simple Ocean Data Assimilation (SODA version 1.4.2) product [*Carton and Giese*, 2008] (see Figure 1). To be consistent with the model depth, the NBL derived from SODA is averaged in the upper 400 m. It can be seen

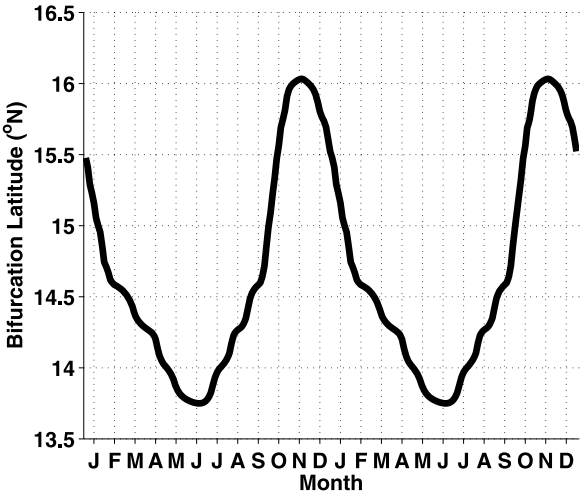

Figure 3. Seasonal variation of the NBL derived from the last 12 years' control run forced by the seasonally varying wind stress of ERA40. The model-simulated bifurcation latitude is plotted for a 2 year period.

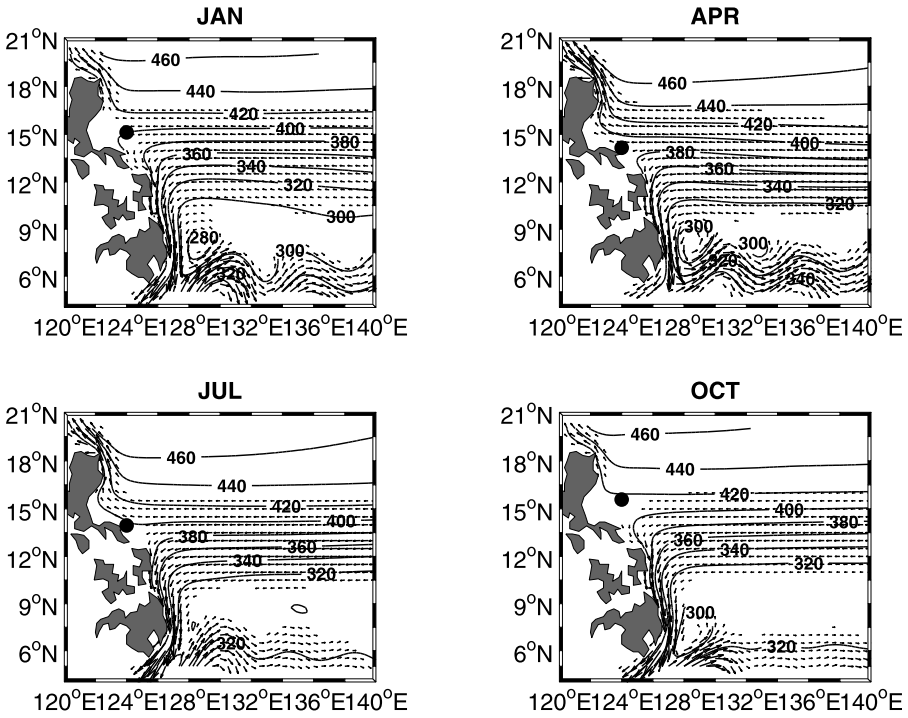

Figure 4. Upper layer thickness (m) and flow (weaker than 10 cm s^{-1} is omitted) in January, April, July, and October. The dot indicates the location of the NEC bifurcation.

that the model-simulated NBL is roughly consistent with that in SODA, although the northward migration in November is more significant in the model.

[14] The circulation pattern in the western Pacific related to the NBL seasonal migration is shown in Figure 4. The NEC bifurcates at around 15°N as encountering the Philippine coast, feeding the northward flowing Kuroshio and southward flowing MC. At 18°N near the Luzon Strait, the Kuroshio intensifies in boreal spring and summer as the NBL moves to its southern position. Similarly, in fall and winter, the Kuroshio is weaker while the NBL tends to be more northward. The seasonal cycle of the Kuroshio transport associated with the NBL is consistent with the observational and modeling studies [*Yaremchuk and Qu*, 2004; *Tozuka et al.*, 2002].

[15] Generally, the 1.5-layer reduced-gravity model used here reasonably captures the major features of the seasonal variations of the upper ocean circulation in the western tropical Pacific especially the NBL seasonal variation both in phase and amplitude. Next we will use this model to further explore the dynamics controlling the seasonal variations of the NBL.

3. Role of Wind Stress Forcing: Extratropics Versus Tropics

[16] The contrast in the amplitude of the NBL seasonal variation between the linear Sverdrup theory prediction and the nonlinear reduced-gravity basin-scale model simulation indicated by QL96 raises the possibility of potential contributions of the nonlocal forcing, particularly the extratropical wind stress forcing to the NBL seasonal variation. In this section, we will assess this impact by conducting a series of numerical experiments.

3.1. Sverdrup Theory Revisited

[17] We first revisit the linear Sverdrup theory using the 1.5-layer nonlinear reduced-gravity model. In general, the NEC should bifurcate along the line of zero wind stress curl as the wind stress forcing is steady, that means, the NBL moves along with the meridional migration of the zero curl line. To test that, a series of perpetual runs are conducted in which the wind stress of each month forces the ocean for 12 years. Results show that the NBL derived from the perpetual runs (the solid dots in Figure 5b) corresponds well with the zonally averaged wind stress curl over the Pacific Ocean (Figure 5a). The south to north migration of the NBL is almost 10°, which is consistent with the amplitude as well as the phase of the averaged zero curl line. The NBL derived from the control run in which the ocean is driven by the seasonally varying wind stress, however, exhibits amplitude of 2°, which accounts for less than 20% of that in the perpetual runs. It has been noted in the study of QL96 that the time taken for the annual Rossby waves to cross the Pacific in the latitudes of bifurcation is around 3 years, so this time-independent Sverdrup theory is not applicable to the NBL on the seasonal time scale. As a result of cancellation between local Ekman pumping and westward propagating Rossby waves, the integral effect on the amplitude of the NBL is small compared with the annual migration of the zonally integrated wind stress curl line. This can be explained by the time-dependent linear wave dynamics (QL96). However, the annual migration of the NBL predicted by the linear wave dynamics appears to be much smaller compared with the 1.5-layer nonlinear reduced-

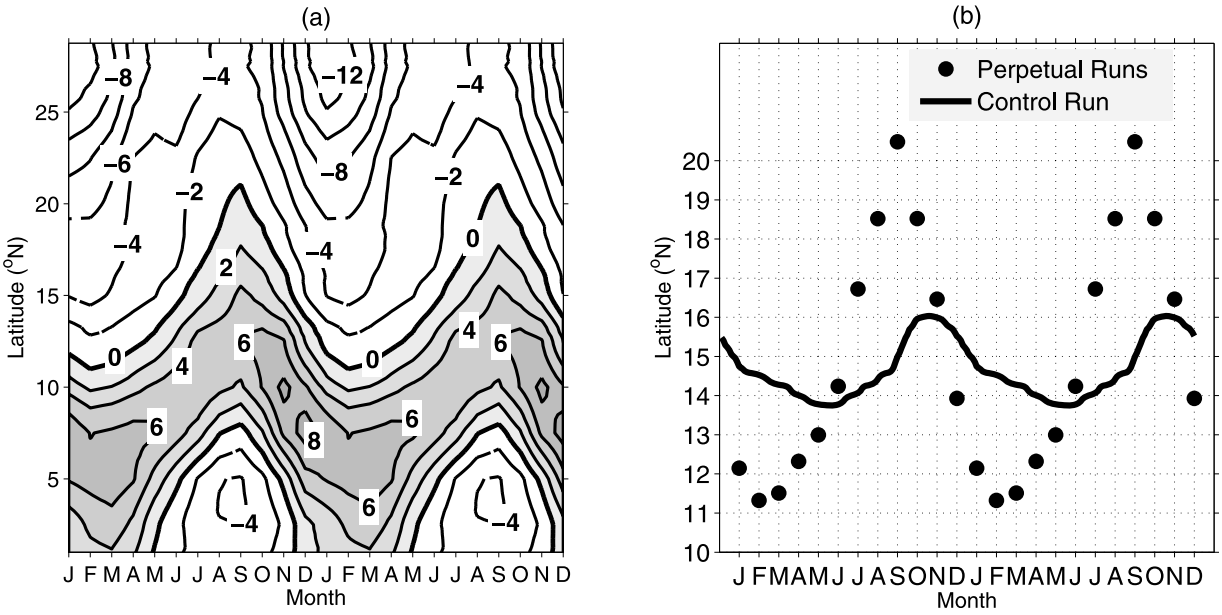

Figure 5. (a) Basin-wide zonally averaged wind stress curl as a function of month (units 10^{-8} Nm^{-3}) derived from ERA40 monthly climatological wind stress. (b) NBL derived from the perpetual runs (solid dots) and the control run (solid line).

gravity model simulation. What are potential reasons for this large amplitude disparity? Next we will focus on the extratropical wind stress which is not included in the linear model.

3.2. Roles of Extratropical Wind Forcing

[18] The linear Sverdrup theory merely considers the wind stress forcing over the tropics in the NBL calculation. In the 1.5-layer reduced-gravity model, however, the wind stress outside the tropics is also included. Indeed, the westward propagating Rossby waves generated at the midlatitudes should be reflected at the western boundary into equatorward propagating CKWs and eastward propagating short Rossby waves. These equatorward propagating CKWs may alter the circulation pattern of the western boundary at lower latitudes and consequently the NBL [*Qu and Lukas*, 2003]. A theory proposed in the previous study [*Liu et al.*, 1999] also shed light on the modulation effect of extratropical oceanic variability on the low-latitude thermocline in an idealized model.

[19] In order to examine the propagation of the CKWs (in this study we refer to the baroclinic CKWs which propagate within the thermocline) and its impact on the circulation near the Philippine coast, we set up an initial spin-up run in which the wind stress anomalies are applied only north of 30°N with no wind stress forcing elsewhere. The propagation of the CKWs is easily identified by the upper layer thickness evolution along the western coast in the first 20 days (Figure 6a) and it requires less than half a month for the CKWs to reach the Philippine coast from extratropics north of 30°N. The seasonal evolution of the upper layer thickness east of Philippines also displays the seasonal signals carried by the CKWs (Figure 6b). The geostrophic calculation in Figure 6c shows that a northward flow exists in the first half of the year while a southward flow in the rest of the year. The northward flow further helps the NBL move to a relative southward position and vice versa. Therefore, the CKW-related flow generated by the seasonal variations of the extratropical wind, though relatively weaker than the background flow field, may modulate the seasonal variation of the NBL.

[20] The experiment above does not include the mean flow. Next we conduct two sensitivity experiments to further assess the potential impacts of the extratropical wind on the NBL seasonal variation. Both runs are the same as the control run, but in the first run with a damping wall placed from the model coast to 140°E at 25°N to block the propagation of the CKWs from the extratropics, and the second run with a climatological wind stress forcing (no seasonal variations) in the extratropical region (north of 25°N). Both experiments aim to remove the influence of the CKWs forced by the seasonal variations of the extratropical wind. It can be seen that the seasonal variation of the NBL derived from these two runs resembles each other in both phase and amplitude, displaying a southernmost latitude in summer and northernmost latitude in winter (Figure 7). Compared with the control run, the most striking difference is a reduction of the amplitude of the northward migration in fall season with phase lagging by about 1 month. Similarly, a slight reduction of southward migration is seen in spring and early summer. Considering the amplification in magnitude caused by the CKWs in the control run, the experiments readily indicate a significant modulation in the north to south migration of the seasonal NBL by the extratropical wind through CKWs.

[21] To further examine the amplification of the seasonal migration of the NBL due to the presence of the CKWs, the alongshore propagation of upper layer thickness anomalies at the western boundary as well as its propagation over the tropical basin is shown in Figure 8. As displayed in Figure 8a,

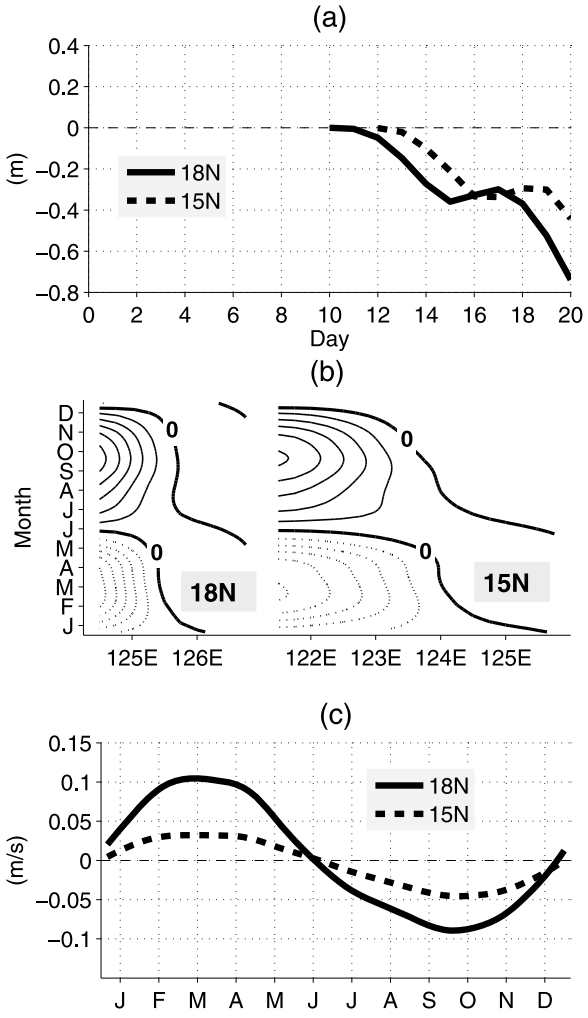

Figure 6. (a) Upper layer thickness anomalies (m) along the Philippine coast at 18°N and 15°N in the first 20 days' spin-up. (b) Seasonal cycle of upper layer thickness anomalies (m) across these two sections. The solid contours denote positive anomalies in the upper layer, while the dashed contours denote negative anomalies. The contour interval is 3 m. (c) Seasonal geostrophic flow across these two sections. The positive value indicates a northward flow.

distinct negative (positive) anomalies of upper layer thickness generate north of 35°N in March (September) and then propagate equatorward along the western boundary. As they are traveling to the low latitudes, intensities of the anomalies decrease due to dissipation. Since the *e*-folding length scale of the baroclinic CKWs is less than 100 km around the bifurcation area, the local circulation especially within 1.5° from the coast is significantly altered with negative anomalies in the first half of the year and positive anomalies in the rest of the year (Figure 8b). In the tropical ocean, the circulation pattern further away from the coast is dominated by the time-dependent linear Rossby wave responses to the wind stress curl field. As shown in Figure 8c, the upper layer thickness anomalies between 126°E and 136°E are dominated by the baroclinic adjustment which attributes to the propagation of the annual Rossby waves in the tropical basin (Figure 8d), and these anomalies are negative (positive) off the western boundary from December to January (June to July). This leads to stronger negative (positive) pressure gradient and thus a stronger southward (northward) flow anomaly in November (June) which is in favor of the amplifications of the NBL annual migration. So it is a phase matching in setting up the pressure gradient between the CKWs near the boundary and the Rossby wave adjustment off the boundary.

[22] The experiments above indicate that the seasonally varying wind stress over the extratropical Pacific nearly accounts for 50% of the total amplitude of the NBL annual migration, and the peak seasons are shifted by 1 month lead due to the presence of the CKWs. To further demonstrate the effect of CKWs from different latitudes, a set of sensitivity runs are conducted. The seasonality of the wind stress is shielded systematically north of certain latitudes from 20°N to 40°N with 5° interval. Thus, we can depict the role of CKWs of different latitudes in comparison with the control run. Figure 9a shows the NBL seasonal variations derived from four sensitivity runs together with the control run. Basically, the amplitude increases as the southern boundary of the shielding area moves northward (Figures 9a and 9b), together with a systematic shift of phase (Figure 9c). The proportion that the CKWs account for the seasonal bifurcation in each sensitivity case can be quantified in terms of skill and correlation (Figure 9d). The skill is defined by $S = 1 - \langle (NBL_{Ctrl} - NBL_{Sen})^2 \rangle / \langle NBL_{Ctrl}^2 \rangle$, where NBL_{Ctrl} is the NBL time series derived from the control run, NBL_{Sen} is the NBL time series derived from each sensitivity run, and the angle brackets denote time averaging [*Qiu*, 2002]. Here we select skill as a proxy to describe the relationship between two time series in comparison to the correlation coefficient. Both skill and correlation display an upward trend along with the increasing shielding latitude, implying that the CKWs generated from different latitudes superimpose their signals on the low-latitude ocean circulation. Evidently, the CKWs generated north of 25°N account for 50% (correlation coefficient 0.7) of the total migration of the NBL in the control

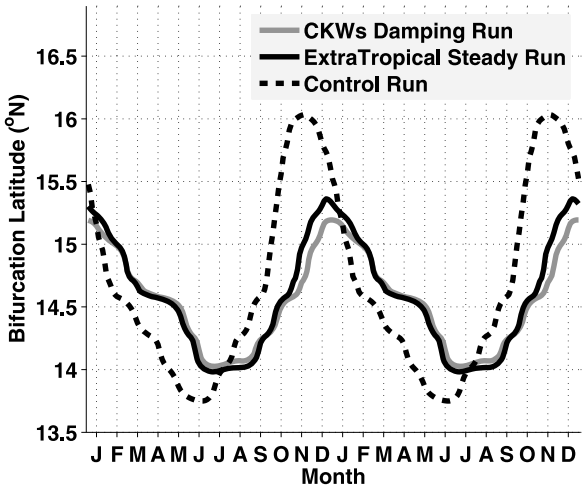

Figure 7. Seasonal variations of the NBL derived from the CKW damping run (gray line), the extratropical steady run (solid black line), and the control run (dashed line). The values are calculated from the last 12 years' integration in each run.

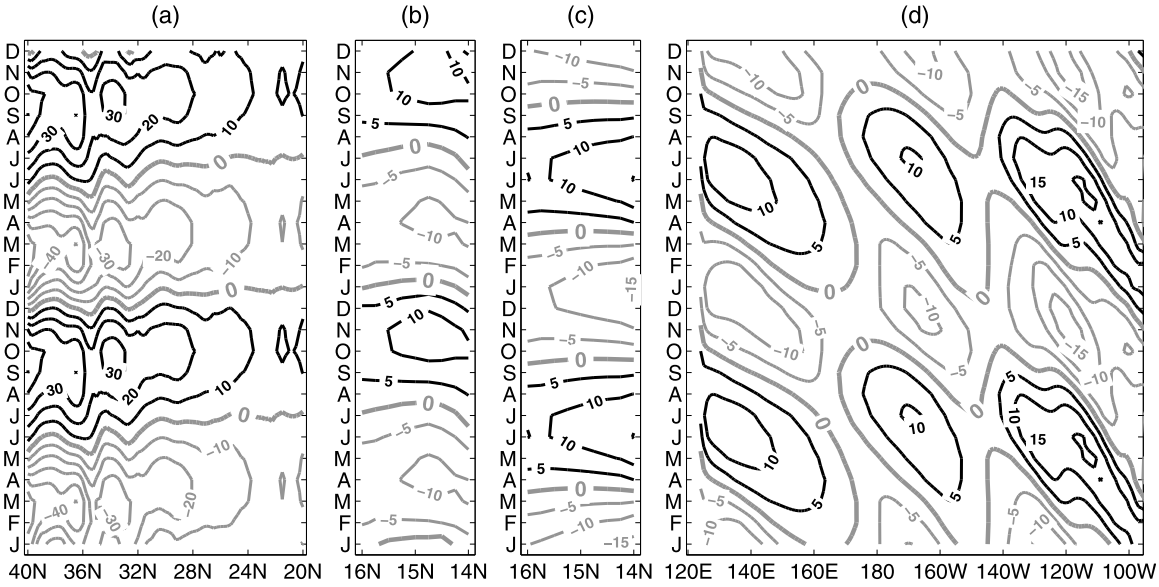

Figure 8. Hövmoller diagram of upper layer thickness anomalies (m) calculated from the last 12 years' control run (a) along the western boundary from 40°N to 20°N, (b) along the Philippine coast within 1.5° width, (c) off the Philippine coast between 126°E and 136°E, and (d) along 15°N. The contours are plotted for a 2 year period for clarity.

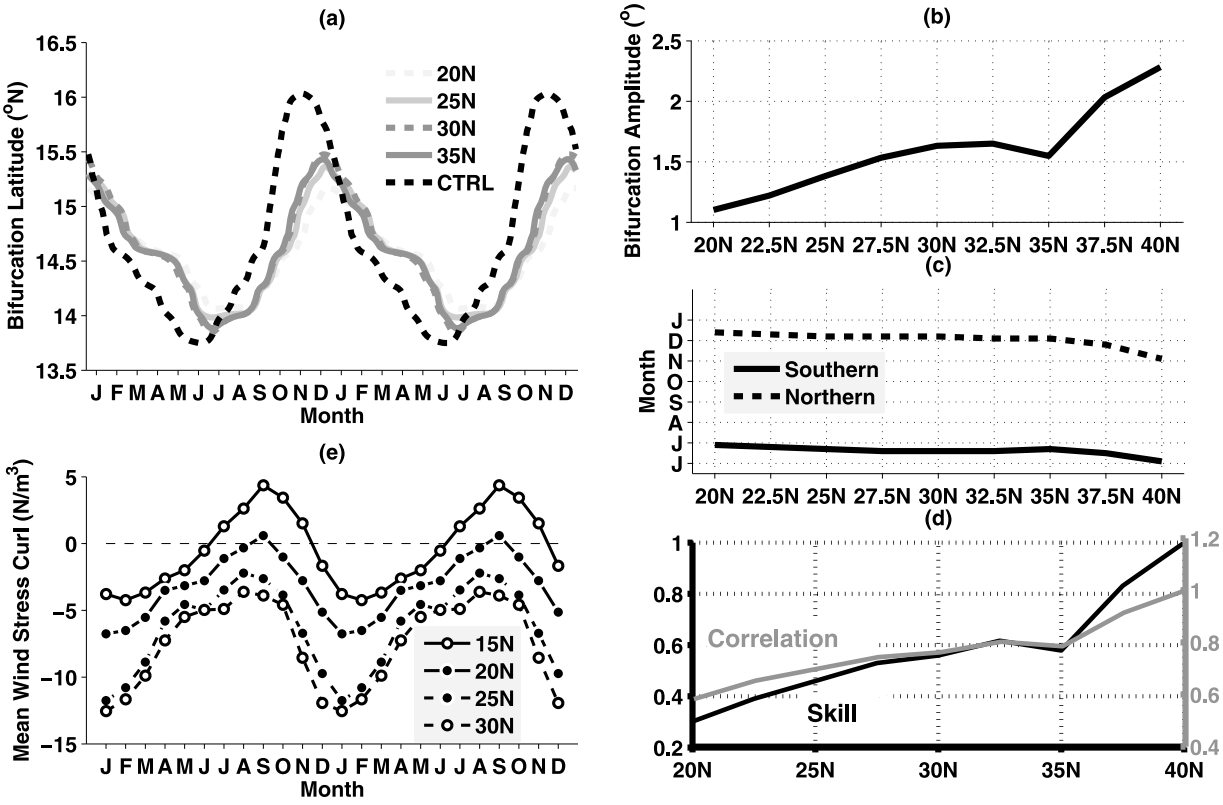

Figure 9. (a) Seasonal variations of the NBL derived from sensitivity runs in which the seasonality of the wind stress is shielded north of certain latitudes from 20°N to 40°N. (b) Annual migration of the NBL derived from the sensitivity runs as a function of latitude. (c) Same as Figure 9b but for the peak seasons in each run. (d) Skill (black line) and correlation (gray line) of the sensitivity runs as a function of latitude. (e) Zonally averaged wind stress curl at different latitudes as a function of month (units 10^{-8} Nm^{-3}) derived from ERA40 monthly climatological wind stress.

run. Traditional view on the NBL seasonal variations mainly emphasizes the wind stress locally over the tropical ocean, and the results shown here suggest the impacts of the extratropical wind stress through CKWs cannot be ignored.

[23] Although the extratropical wind exerts significant impacts on the NBL annual migration, the phase of the NBL seasonal variation is predominantly determined by the wind stress in the tropics, with a minor modulation by extratropical forcing. The 1 month lead is largely due to a fast propagation of the CKWs (less than a month) as well as the phase lag of the wind stress seasonal variations toward lower latitudes (Figure 9e).

4. Role of Baroclinic Rossby Wave Propagation

[24] Since the phase of the NBL seasonal variation is predominantly determined by the wind stress in the tropics, the linear wave dynamics should be able to capture the phase of the observed NBL seasonal variation. The key dynamic process in the linear Sverdrup model is the first-mode baroclinic Rossby wave propagation [*Meyers*, 1979], with phase speed determined by both background stratification and thermocline depth. In this section, we will explore how the first-mode baroclinic Rossby wave propagation affects the NBL seasonal variation.

4.1. The First-Mode Baroclinic Rossby Wave Dynamics of the NBL Revisited

[25] To establish the relationship between the fluctuations of the surface wind field and the NBL, QL96 used linear wave dynamics in which they constructed a formula to represent the seasonally fluctuating wind stress curl field. Instead of using a zonally uniform wind stress curl as QL96, here we adopt the realistic wind stress curl field to force a linear, first-mode baroclinic Rossby wave model, which can be expressed as

$$\frac{\partial h}{\partial t} + C_R \frac{\partial h}{\partial x} = -\frac{1}{\rho} \nabla \times \left(\frac{\boldsymbol{\tau}}{f} \right) - \varepsilon h, \tag{4}$$

where h is the upper layer thickness deviation from the mean upper layer thickness H, f the Coriolis parameter, ρ the mean density, $\boldsymbol{\tau}$ the vector of surface wind stress and ε the Newtonian dissipation rate with the unit of yr^{-1} (in this study we choose $\varepsilon = 0$ in order to compare with the results of QL96). Note that $C_R = -(\beta c^2/f^2)$ is the phase speed of the first-mode baroclinic Rossby waves and negative sign denotes a westward propagation, where β is the meridional gradient of f and $c = (g'H)^{1/2}$ the phase speed of the internal gravity waves. Integrating the above equation from the eastern boundary along the baroclinic Rossby wave characteristic line ($x - C_R t = const$) yields solution as

$$h(x,y,t) = -\frac{1}{\rho f} \int_{x_e}^{x} \frac{1}{C_R} curl\boldsymbol{\tau} \left(x', y, t + \frac{x' - x}{C_R} \right) \times \exp\left[\frac{\varepsilon (x' - x)}{C_R} \right] dx', \tag{5}$$

in which the contribution from the eastern boundary has been ignored [*Cabanes et al.*, 2006; *Zhang and Wu*, 2010]. Note that C_R is also a function of longitude in view of the thermocline tilting from west to east, and it is chosen from 0.1 m s^{-1} in the eastern Pacific to 0.2 m s^{-1} in the western basin around the bifurcation region by following *Chelton et al.* [1998]. The mean C_R is about 0.15 m s^{-1}, which is consistent with that in the 1.5-layer reduced-gravity model. The wind stress curl is calculated from the ERA40 monthly climatological wind stress.

[26] The linear wave model reasonably captures the observed phase of the NBL seasonal variation (Figure 10), similar to the results as the CKWs from the extratropics in the numerical model are shielded, except for slight differences in the amplitude which may be due to the absence of nonlinearity and the negligence of the detailed flow structure inside the western boundary [*Qiu and Lukas*, 1996]. This is in contrast to that of QL96, providing a further support for the controlling of the linear Rossby wave dynamics on the phase of the NBL seasonal variations.

4.2. Role of Wave Speed

[27] Why is the prediction of the linear wave model here different from that of QL96? In the study of QL96, the seasonal NBL predicted by their linear model is well represented by an analytic expression. The synthetic expression of wind stress curl, however, excludes significant effect of the Southeast Asian monsoon east of Philippines. Moreover, the propagation speed of the first-mode Rossby wave C_R is a constant as suggested in the study of QL96. These assumptions may lead to deviation of the linear Sverdrup theory prediction from the observation. To compare the performances of these two linear models in reproducing the seasonal cycle of the NBL and its dependence on the C_R, we extend the range of C_R in the linear models and to assess its impacts on the NBL seasonal variation.

[28] For the north to south migration of the NBL, both models demonstrate an amplifying trend along with the increasing C_R, suggesting the dependence of cancellation between the local Ekman pumping and the westward propagating Rossby waves on different C_R (Figures 11a and 11b). This can be physically interpreted by the fact that less cancellation occurs if the Rossby waves travel fast. The peak seasons in the two models, however, are not linearly correlated with C_R. If the realistic wind stress curl is employed and the C_R is set to be longitude-dependent, the peak season in its northernmost position always maintains in January and slightly fluctuates between July and October in its southernmost position (Figure 11c). This property of phase locking with varying C_R is quite different from that in the model of QL96 which is largely dependent on C_R (Figure 11d). For instance, the northernmost (southernmost) position occurs in December (June) when C_R is 13 cm s^{-1} while it is in July (January) when C_R is 19 cm s^{-1}.

[29] To further explore the first-mode Rossby wave propagation speed in determining the NBL seasonal variation, we use the 1.5-layer nonlinear model through a systematic change of the stratification. As shown in Figure 12, the amplitude of the seasonal bifurcation increases as the stratification of the ocean intensifies within the 10°N–20°N tropical band, consistent with the linear wave model prediction. In this case, the annual migration can reach 4° as the density contrast between the upper layer and the infinite deep layer becomes larger, which implies that less cancellation takes place due to larger phase speed. The phase,

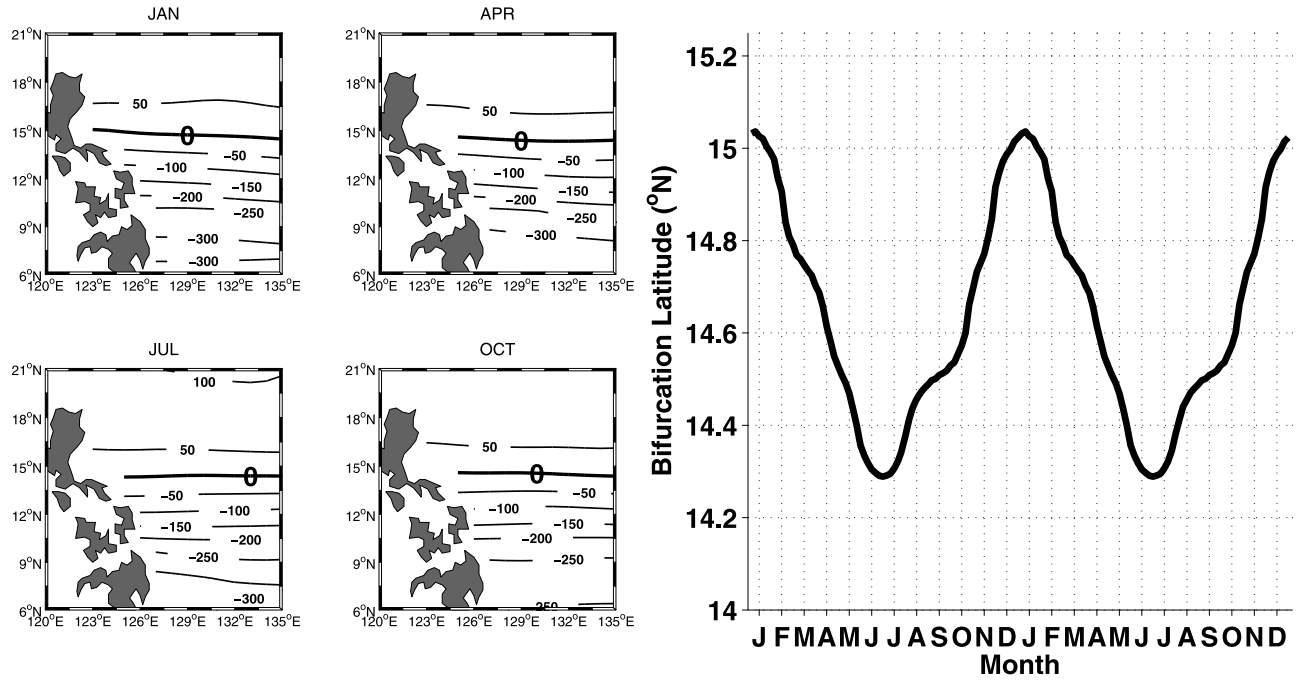

Figure 10. (left) Upper layer thickness anomalies (units m) predicted by the linear, first-mode baroclinic Rossby wave model in January, April, July, and October. (right) Seasonal variation of the NBL derived from the upper layer thickness anomalies.

however, has no significant shift in its northernmost position as the linear result shows in Figure 11c. Both of the results in the linear model and the 1.5-layer reduced-gravity model raise the possibility that the wind stress curl is more important than C_R in determining the phase of the NBL seasonal variation. In section 4.3 we will further address the roles of local and remote forcing in controlling the phase of the seasonal NBL.

4.3. Role of Local Forcing

[30] To further assess the role of local/remote wind stress forcing in the seasonal NBL, we eliminate the seasonality of the wind stress curl west of 135°E (local fix case) and east of 135°E (remote fix case) to force the linear model with varying C_R from 15 cm s^{-1} to 25 cm s^{-1}. In the absence of local seasonal forcing, both amplitude and phase display a nonlinear behavior as mean C_R increases (Figures 13a and 13c). However, in the presence of the local seasonal forcing, the northward migration increases monotonically while the southward migration remains virtually unchanged. Furthermore, the peak phase of the northward migration remains stable and the southward migration occurs systematically earlier with increasing C_R. All these features have pointed to the important role of the local seasonal forcing in locking the phase of the NBL seasonal variation.

[31] We also performed sensitivity experiments using the method of *Qiu and Chen* [2010] to verify the above conclusion. In the linear wave model, if we use the steady wind stress curl between the Philippine coast (120°E) to a certain longitude continuously until the eastern boundary with 10° interval, the correlation between the control case and the sensitivity cases decreases (Figure 14), indicating the crucial role of local wind (Southeast Asian monsoon) forcing in determining the phase of the seasonal NBL.

5. Discussion

[32] Although the 1.5-layer model reasonably captures the observed seasonal cycle, it possibly overestimates the influences of the CKWs because the model ignores the marginal seas as well as shallow straits in the western Pacific and provides a straight path for the CKWs to the tropics.

5.1. Sensitivity to Closed or Open Luzon Strait

[33] To assess how the above results are sensitive to whether the Luzon Strait is closed or open, we extend the model domain to the west to include the entire SCS. In addition to the control run (forced by the monthly climatological wind stress), the seasonality of the wind stress is shielded north of 25°N as we did in the sensitivity runs in section 3.2. Results show that the seasonal variation of the NBL in this larger domain displays peak-to-peak amplitude of 1.6°, less than the control run in which the SCS and the Luzon Strait are excluded (Figure 15). For the sensitivity run, the north to south migration of the NBL is reduced by more than 35% of that in the control run, which is comparable to the reduction as the Luzon Strait is closed. Therefore, the conclusions derived from the previous modeling studies remain robust.

5.2. OGCM Experiment

[34] It still remains uncertain whether the conclusion that the extratropical wind stress impacts on the NBL seasonal variation derived from the above simple model studies is applicable to the realistic ocean. In general, it is difficult to

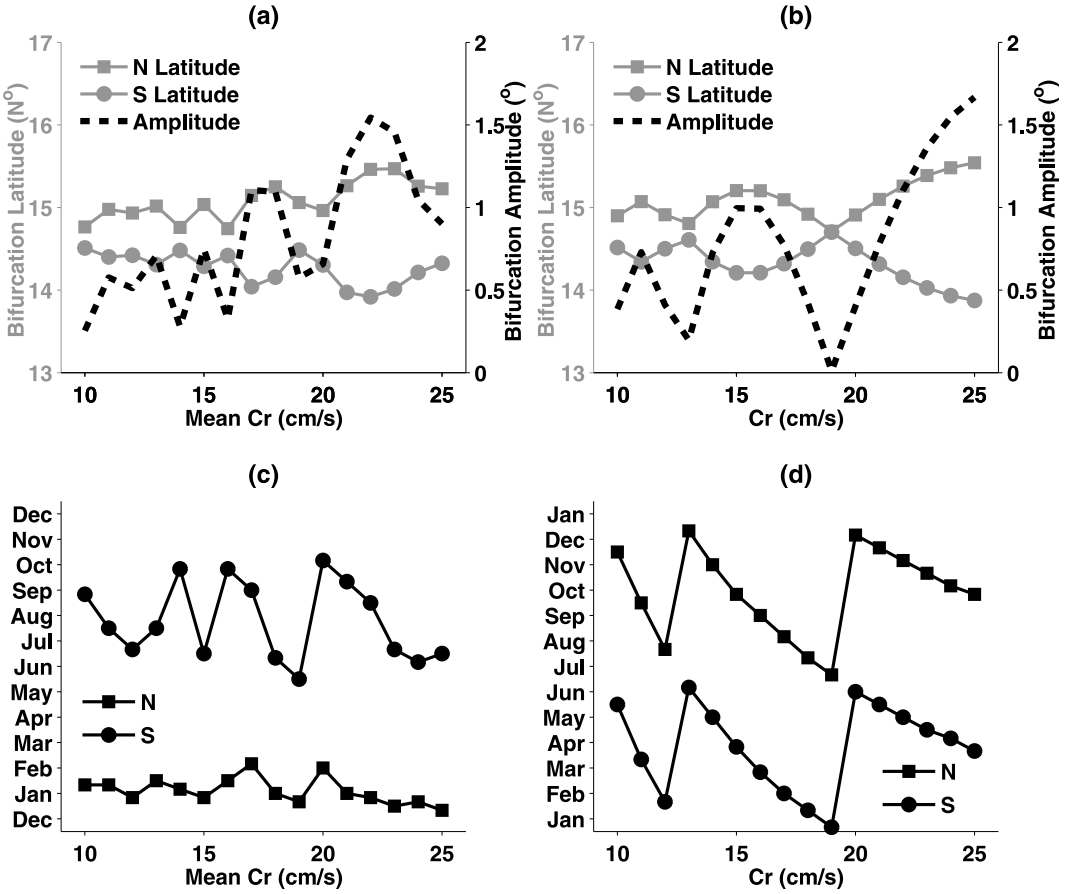

Figure 11. (a) Northernmost (southernmost) bifurcation latitude and the amplitude as a function of mean C_R predicted by the linear, first-mode baroclinic Rossby wave model. (b) Same as Figure 11a but by the synthetic expression provided by QL96. (c) Peak seasons as a function of mean C_R predicted by linear, first-mode baroclinic Rossby wave equation. (d) Same as Figure 11c but by the synthetic expression provided by QL96.

diagnose the influences of the extratropical winds on the NBL migration from the observations. Here we adopt the Modular Ocean Model version 4.1 (MOM4p1) developed by Geophysical Fluid Dynamics Laboratory (GFDL) to validate the linear wave dynamics in controlling the NBL seasonal variation. The model adopts locally high resolution refinement grid with horizontal resolution 0.25° × 0.25° with 32 levels in the vertical direction in the region (30°S–75°N) and (30°E–70°W). Outside of this region, the model's resolution is 5° by 5°. The model is forced by the Common Ocean-ice Reference Experiments (CORE) data set [*Large and Yeager*, 2004]. It is driven by the climatological forcing for 30 years to reach a quasi-equilibrium state. After that, a control run is conducted with forcing spanning from 1985 to 2005. To assess the influences of the extratropical wind variations on the NBL, a sensitivity experiment is conducted in which the seasonal variations of the wind north of 25°N over the Pacific Ocean is shielded from 2001 to 2005.

[35] The seasonal variation of the NBL in the upper 400 m derived from the control run resembles the observed results, which reaches its southernmost position in June/July and northernmost position in November (Figure 16a). The amplitude of the seasonal migration is about 0.8°–0.9°,

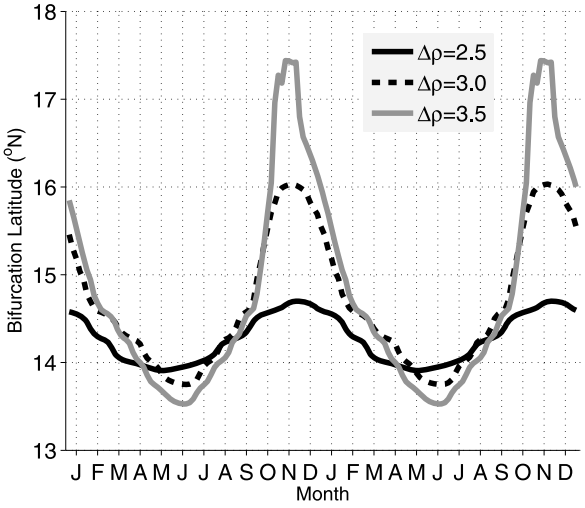

Figure 12. Seasonal variation of the NBL derived from sensitivity runs in which different stratifications are selected within the 10°N–20°N tropical band.

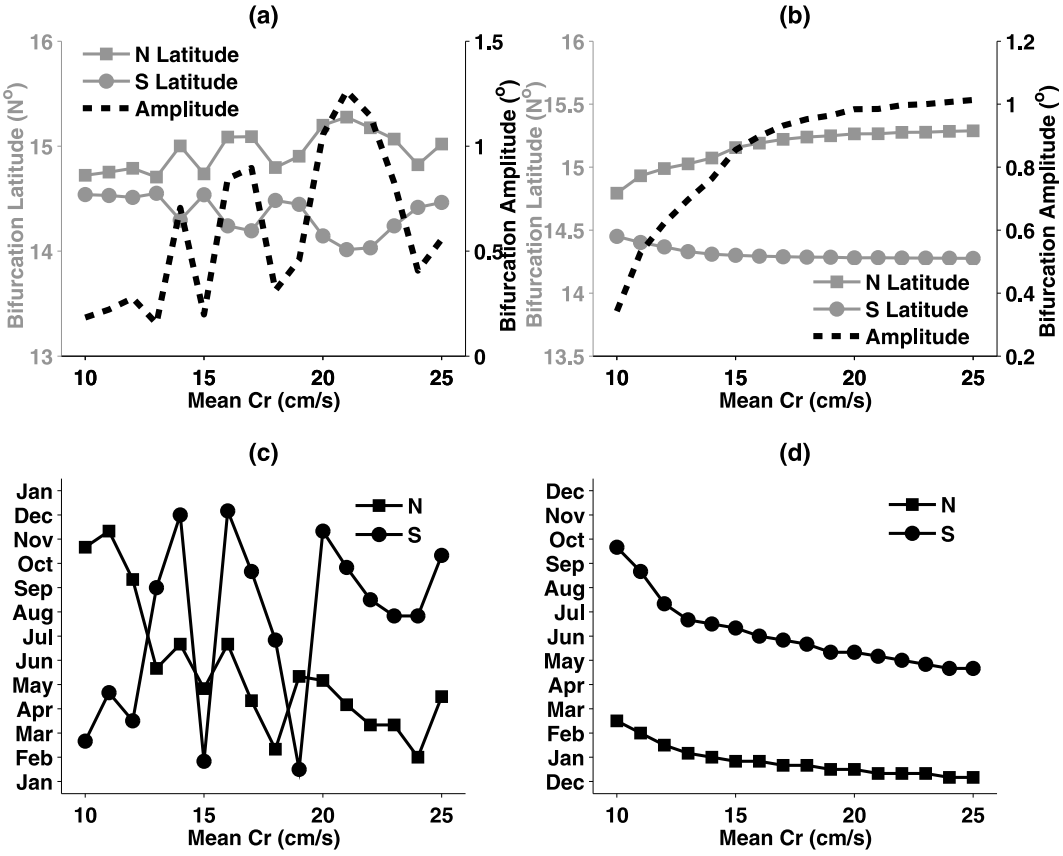

Figure 13. Same as Figure 11 but with the seasonality of wind stress curl in (a, c) the local basin (120°E–135°E, 6°N–21°N) and (b, d) the remote basin (135°E to eastern boundary, 6°N–21°N) removed. Results are derived from the linear, first-mode baroclinic Rossby wave model.

which is at the lower end of the observations. Consistent with observations, the NBL in the model shifts northward with depth (Figure 16b). As the seasonal variations of the extratropical wind are suppressed, the peak-to-peak amplitude of the NBL migration is reduced by about 30% (from 0.9° to 0.6°), although the mean NBL is southward shifted by about 0.3° (Figure 16a). This is consistent with these of the 1.5-layer model simulation. Since the OGCM is more complex and involves many different processes, more studies with OGCM will be done in the future to further quantify different impacts, for instance, heat and freshwater forcing, and influences from the Southern Hemisphere.

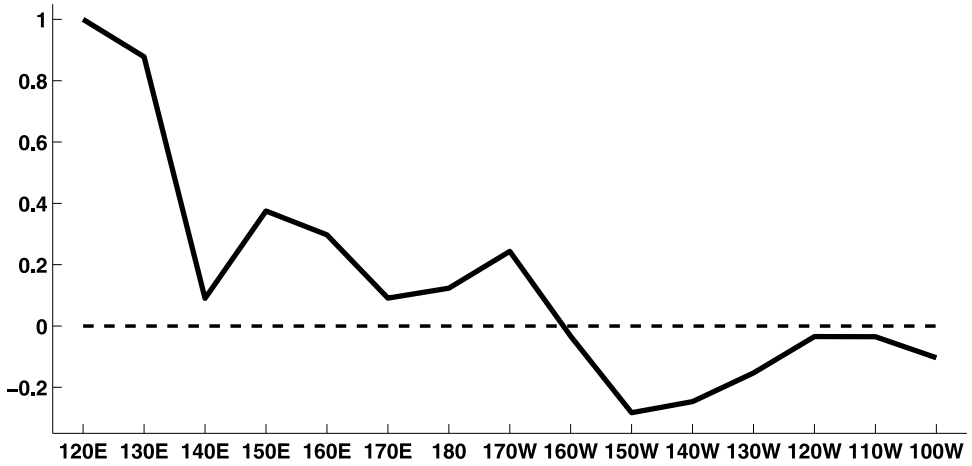

Figure 14. Correlation as a function of longitude calculated from the sensitivity cases in the linear, first-mode baroclinic Rossby wave model.

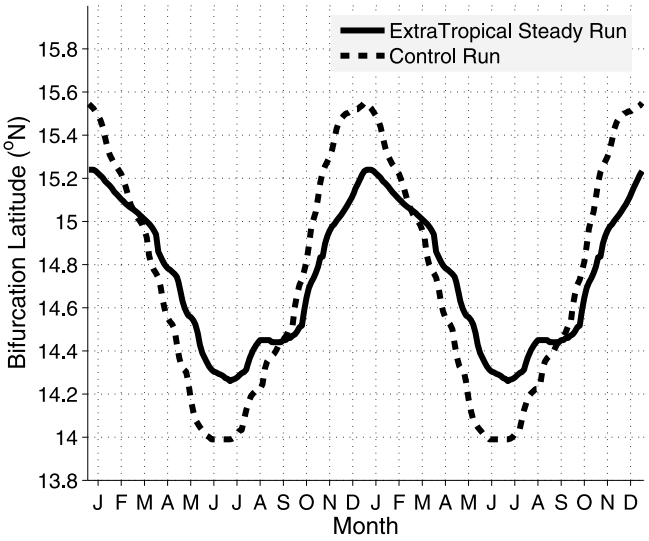

Figure 15. Seasonal variation of the NBL derived from the last 12 years' control run (dashed line) and the extratropical steady run (solid line). The model domain includes the South China Sea with the Luzon Strait connecting to the Pacific Ocean.

5.3. Nonlinearity

[36] Another difference between the linear wave model and the 1.5-layer reduced gravity model is the nonlinearity. A convenient way to assess the role of nonlinearity in the NBL seasonal variation is to eliminate the advection terms in the model. As seen in Figure 17a, the nonlinearity does not modulate the seasonal cycle significantly, but shifts the mean NBL equatorward by about 0.3°–05°. The season at its southernmost in the linear run seems to be earlier than that in the control run while they share the same season at their northernmost position. This is associated with a positive anomaly of the upper layer thickness around the bifurcation region (the dashed rectangle in Figure 17b), which produces an anomalous anticyclonic flow to move the NBL southward. Compared with the extratropical wind forcing, although the effect of the nonlinearity on the NBL seasonal variation is relatively weaker, its role in the western boundary dynamics need to be studied in detail in future.

6. Summary

[37] In the present study, we adopt a 1.5-layer nonlinear reduced-gravity Pacific basin model and a linear, first-mode baroclinic Rossby wave model to investigate the dynamics of the seasonal variation of the NBL. We highlight the important roles of the extratropical wind variations on the seasonal variation of the NBL through CKWs. It is demonstrated that the seasonal north to south migration of the NBL is amplified by the presence of CKWs generated by the extratropical winds with slight phase modulation.

[38] It is found that the time-independent Sverdrup theory can explain the NBL at the western boundary if the wind stress forcing is steady. Cancellation between local Ekman pumping and the westward propagating anomalies becomes effective if the wind stress over the tropical Pacific Ocean varies seasonally since the time taken for annual Rossby waves to cross the Pacific in the latitudes of the NEC bifurcation is around 3 years. Therefore, on decadal and longer time scales, the NBL migration may be largely governed by the Sverdrup dynamics.

[39] The model further demonstrates that the amplitude of the NEC bifurcation is also associated with stratification. A strong (weak) stratification leads to a fast (slow) propagation of the first-mode baroclinic Rossby waves. This has an important implication for the NBL changes in global warming. In a warm climate, the oceanic stratification is intensified due to fast warming in the upper ocean, which shall increase the deformation radius of baroclinic Rossby wave and thus accelerate the phase speed. Several studies also have focused on this increasing Rossby deformation radius

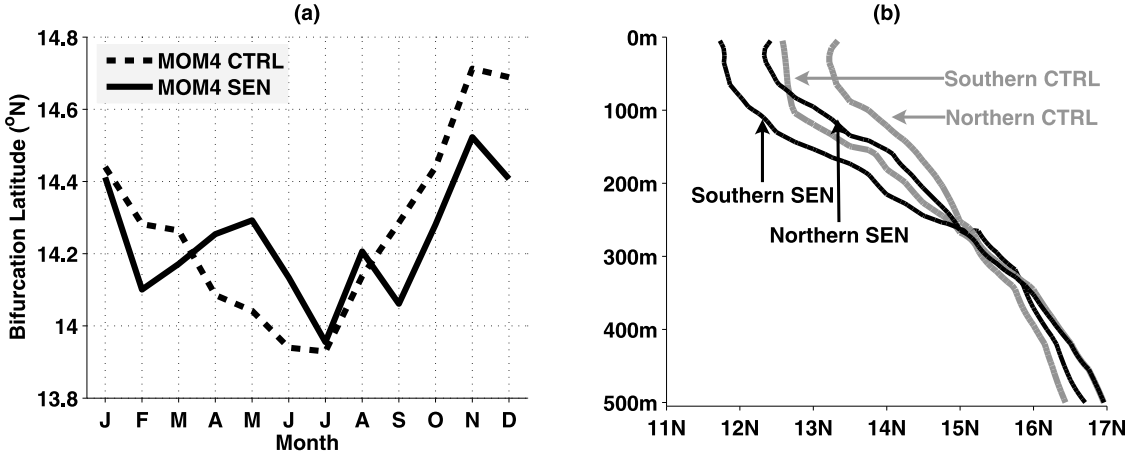

Figure 16. (a) Seasonal NBL in the upper 400 m derived from MOM4 control run (dashed line) and MOM4 sensitivity run (solid line). (b) Zero contours of meridional velocity averaged within a 2° band off the Philippine coast. The gray contours denote the composite bifurcation at its southernmost (northernmost) position in the control run from 2001 to 2005, and the black contours are that in the sensitivity run from 2001 to 2005.

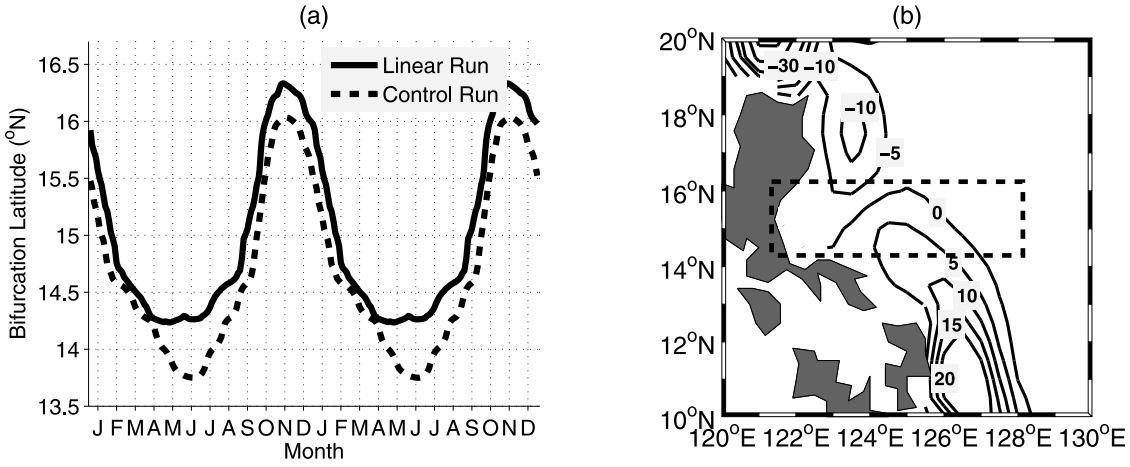

Figure 17. (a) Comparison between the NBL seasonal variations derived from the linear run (solid line) and the control run (dashed line) from the last 12 years' simulation. (b) Mean upper layer thickness anomalies (control run minus linear run, units m).

(by 5%–20%) and its potential effects under the scenarios of global warming [*Saenko*, 2006; *Sueyoshi and Yasuda*, 2009]. It will be expected that the annual migration of the NBL will be amplified in the 21st century as the greenhouse gases elevate. This amplification of the NBL may lead to redistribution of the water mass and heat transport along the western boundary, and thus warm pool and monsoon climate.

[40] **Acknowledgments.** This work is supported by the Major Project of National Science Foundation of China (40890150, 40890155) and the Chinese National Key Basic Research Program (2007CB411800). We are very grateful to the two anonymous reviewers for their constructive comments. Discussions with Bo Qiu and Dunxin Hu are greatly appreciated. We are also in indebted to Chengyan Liu for providing us the MOM4 simulation used in this study.

References

Antonov, J. I., D. Seidov, T. P. Boyer, R. A. Locarnini, A. V. Mishonov, and H. E. Garcia (2010), *World Ocean Atlas 2009*, vol. 2, *Salinity*, *NOAA Atlas NESDIS*, vol. 69, edited by S. Levitus, 184 pp., NOAA, Silver Spring, Md.

Cabanes, C., T. Huck, and A. C. D. Verdiere (2006), Contributions of wind forcing and surface heating to interannual sea level variations in the Atlantic Ocean, *J. Phys. Oceanogr.*, *36*, 1739–1750, doi:10.1175/JPO2935.1.

Carton, J. A., and B. S. Giese (2008), A reanalysis of ocean climate using simple ocean data assimilation (SODA), *Mon. Weather Rev.*, *136*, 2999–3017, doi:10.1175/2007MWR1978.1.

Chelton, D. B., and M. G. Schlax (1996), Global observations of oceanic Rossby waves, *Science*, *272*, 234–238, doi:10.1126/science.272.5259.234.

Chelton, D. B., R. A. de Szoeke, M. G. Schlax, K. E. Naggar, and N. Siwertz (1998), Geographical variability of the first baroclinic Rossby radius of deformation, *J. Phys. Oceanogr.*, *28*, 433–460, doi:10.1175/1520-0485(1998)028<0433:GVOTFB>2.0.CO;2.

Kim, Y. Y., T. Qu, T. Jensen, T. Miyama, H. W. Kang, H. Mitsudera, and A. Ishida (2004), Seasonal and interannual variations of the North Equatorial Current bifurcation in a high-resolution OGCM, *J. Geophys. Res.*, *109*, C03040, doi:10.1029/2003JC002013.

Large, W., and S. Yeager (2004), Diurnal to decadal global forcing for ocean and sea-ice models: The data sets and flux climatologies, *Tech. Note TN-460+STR*, 105 pp., Natl. Cent. for Atmos. Res., Boulder, Colo.

Liu, Z., L. Wu, and E. Bayler (1999), Rossby wave-coastal Kelvin wave interaction in the extratropics. Part I: Low frequency adjustment in a closed basin, *J. Phys. Oceanogr.*, *29*, 2382–2404, doi:10.1175/1520-0485(1999)029<2382:RWCKWI>2.0.CO;2.

Locarnini, R. A., A. V. Mishonov, J. I. Antonov, T. P. Boyer, and H. E. Garcia (2010), *World Ocean Atlas 2009*, vol. 1, *Temperature*, *NOAA Atlas NESDIS*, vol. 68, edited by S. Levitus, 184 pp., NOAA, Silver Spring, Md.

Lukas, R., T. Yamagata, and J. P. McCreary (1996), Pacific low-latitude western boundary currents and the Indonesian throughflow, *J. Geophys. Res.*, *101*, 12,209–12,216, doi:10.1029/96JC01204.

Masumoto, Y., and T. Yamagata (1991), Response of the western tropical Pacific to the Asian winter monsoon: The generation of the Mindanao Dome, *J. Phys. Oceanogr.*, *21*, 1386–1398, doi:10.1175/1520-0485(1991)021<1386:ROTWTP>2.0.CO;2.

Meyers, G. (1979), On the annual Rossby wave in the tropical North Pacific Ocean, *J. Phys. Oceanogr.*, *9*, 663–674, doi:10.1175/1520-0485(1979)009<0663:OTARWI>2.0.CO;2.

Nitani, H. (1972), Beginning of the Kuroshio, in *Kuroshio: Its Physical Aspects*, edited by H. Stommel and K. Yoshida, pp. 129–163, Univ. of Tokyo Press, Tokyo.

Qiu, B. (2002), Large-scale variability in the midlatitude subtropical and subpolar North Pacific Ocean: Observations and causes, *J. Phys. Oceanogr.*, *32*, 353–375, doi:10.1175/1520-0485(2002)032<0353:LSVITM>2.0.CO;2.

Qiu, B., and S. Chen (2010), Interannual-to-decadal variability in the bifurcation of the North Equatorial Current off the Philippines, *J. Phys. Oceanogr.*, *40*, 2525–2538, doi:10.1175/2010JPO4462.1.

Qiu, B., and R. Lukas (1996), Seasonal and interannual variability of the North Equatorial Current, the Mindanao Current and the Kuroshio along the Pacific western boundary, *J. Geophys. Res.*, *101*, 12,315–12,330, doi:10.1029/95JC03204.

Qu, T., and R. Lukas (2003), The bifurcation of the North Equatorial Current in the Pacific, *J. Phys. Oceanogr.*, *33*, 5–18, doi:10.1175/1520-0485(2003)033<0005:TBOTNE>2.0.CO;2.

Qu, T., H. Mitsudera, and T. Yamagata (1998), On the western boundary currents in the Philippine Sea, *J. Geophys. Res.*, *103*, 7537–7548, doi:10.1029/98JC00263.

Reid, J. L., and R. S. Arthur (1975), Interpretation of maps of geopotential anomaly for the deep Pacific Ocean, *J. Mar. Res.*, *33*, 37–52.

Rodrigues, R. R., L. M. Rothstein, and M. Wimbush (2007), Seasonal variability of the South Equatorial Current bifurcation in the Atlantic Ocean: A numerical study, *J. Phys. Oceanogr.*, *37*, 16–30, doi:10.1175/JPO2983.1.

Saenko, O. A. (2006), Influence of global warming on baroclinic Rossby radius in the ocean: A model intercomparison, *J. Clim.*, *19*, 1354–1360, doi:10.1175/JCLI3683.1.

Sueyoshi, M., and T. Yasuda (2009), Reproducibility and future projection of the ocean first baroclinic Rossby radius based on the CMIP3 multi-model dataset, *J. Meteorol. Soc. Jpn.*, *87*(4), 821–827, doi:10.2151/jmsj.87.821.

Toole, J. M., E. Zou, and R. C. Millard (1988), On the circulation of the upper waters in the western equatorial Pacific Ocean, *Deep Sea Res.*, *35*(9), 1451–1482, doi:10.1016/0198-0149(88)90097-0.

Toole, J. M., R. C. Millard, Z. Wang, and S. Pu (1990), Observations of the Pacific North Equatorial Current bifurcation at the Philippine coast, *J. Phys. Oceanogr.*, *20*, 307–318, doi:10.1175/1520-0485(1990)020<0307:OOTPNE>2.0.CO;2.

Tozuka, T., T. Kagimoto, Y. Masumoto, and T. Yamagata (2002), Simulated multiscale variations in the western tropical Pacific: The Mindanao Dome revisited, *J. Phys. Oceanogr.*, *32*, 1338–1359, doi:10.1175/1520-0485(2002)032<1338:SMVITW>2.0.CO;2.

Wang, Q., and D. Hu (2006), Bifurcation of the North Equatorial Current derived from altimetry in the Pacific Ocean, *J. Hydrodyn.*, *18*(5), 620–626, doi:10.1016/S1001-6058(06)60144-3.

Wyrtki, K. (1961), *Physical Oceanography of the Southeast Asian Waters*, vol. 2, 195 pp., Scripps Inst. of Oceanogr., Univ. of Calif., San Diego, La Jolla.

Yaremchuk, M., and T. Qu (2004), Seasonal variability of the large-scale currents near the coast of the Philippines, *J. Phys. Oceanogr.*, *34*, 844–855, doi:10.1175/1520-0485(2004)034<0844:SVOTLC>2.0.CO;2.

Zhang, H., and L. Wu (2010), Predicting North Atlantic sea surface temperature variability based on the first-mode baroclinic Rossby wave model, *J. Geophys. Res.*, *115*, C09030, doi:10.1029/2009JC006017.

Z. Chen and L. Wu, Physical Oceanography Laboratory, Ocean University of China, 238 Songling Rd., Qingdao 266100, China. (chenzhaohui@ouc.edu.cn)